Seismic Hazard Inferred from Tectonics: California

Peter Bird and Zhen Liu[1]
Department of Earth and Space Sciences, University of California-Los Angeles

INTRODUCTION

In this paper we propose simple methods for estimating long-term average seismicity of any region, based on a local kinematic model of surface velocities and an existing global calibration of plate-boundary seismicity. We apply the method to California and obtain a long-term forecast of seismicity that exceeds the levels seen in several 20th-century catalogs.

This contribution is the third in a series describing a project informally known as Seismic Hazard Inferred from Tectonics (SHIFT). Its goal is to realize the promise of plate tectonic theory to provide long-term seismicity forecasts (and, eventually, seismic hazard forecasts) more reliable than those based primarily on local instrumental and/or historic records. Bird (2003) reviewed the literature on plate tectonics, assembling model PB2002 consisting of 52 plates and 13 orogens, with every plate-boundary step (great-circle arc between digitized points) classified as one of seven types. Bird and Kagan (2004) used this model to assign 95% of shallow earthquakes to appropriate plate boundaries and to estimate the seismicity parameters (width, productivity, spectral slope, corner magnitude, and coupled thickness) for each boundary type. Here we propose simple hypotheses predicting the long-term shallow seismicity produced by any geometry of tectonic faults (and/or zones of distributed anelastic straining) by treating each fault or region as a small sample of the most appropriate type of plate boundary. This is consistent with the observation that the distribution of plate sizes obeys a power law (Bird 2003; Sornette and Pisarenko 2003), so that the number of plates is uncountable, and it may even be difficult to defend a fundamental distinction between plate boundaries and plate interiors in some cases.

To participate in the Regional Earthquake Likelihood Models (RELM) program of testing seismicity forecasts for the California region (Schorlemmer *et al.* 2007, this issue), we compute a long-term forecast based on a kinematic model of neotectonics derived from a weighted least-squares fit to available data. Although the input data sets for the kinematic model are known to have certain deficiencies, and revised kinematic models are planned for the future, these local details are not expected to affect the overall seismicity levels emphasized in this contribution. For example, in a test where we replaced all of the complex fault systems of the California-Nevada region (31.5~43°N, 113.1~125.4°W) with highly simplified plate boundaries from PB2002, the forecast seismicity rate for the region as a whole decreased by only 15% (although the map pattern was very different). This stability results from the strong constraint of fixed Pacific/North America relative rotation.

SEISMICITY OF FAULTS

For any discrete fault with long-term average slip rate $\dot{s}$ (possibly varying in space), the long-term average seismic moment rate is

$$\dot{M}_0 = \iint c\,\mu\,\dot{s}\,\mathrm{d}a \qquad (1)$$

where c is the dimensionless seismic coupling (the fraction of frictional sliding that occurs in earthquakes), μ is the elastic shear modulus, da is an element of fault area, and the integral is over the frictional (potentially seismogenic) portion of the fault surface that lies above the brittle/ductile transition. For large blocks of lithosphere, which do not rotate about horizontal axes (although they may rotate about vertical axes), slip rates hardly vary in the down-dip direction, so we may approximate

$$\dot{M}_0 \cong \langle c\,z \rangle \int \mu \sqrt{v_p^2 + \left(v_o \sec(\theta)\right)^2}\,\csc(\theta)\,\mathrm{d}\ell \qquad (2)$$

where brackets $\langle\ \rangle$ indicate a mean value, z is the potentially seismogenic depth range (depth to the brittle/ductile transition), v_p is the trace-parallel component of the horizontal relative block velocity vector, v_o is the orthogonal (trace-normal) component of the horizontal relative block velocity vector, θ is the fault dip, $\mathrm{d}\ell$ is a small step along the length of the fault, and the integral is taken on the surface along the trace. In this form, we see the importance of the "mean coupled seismogenic thickness" $\langle c\,z \rangle$. Because only the product is used in most computations, it is usually not necessary to separate its two components. We propose that long-term seismic moment rates of faults can be computed using the coupled seismogenic thickness of the most comparable type of plate boundary, with assignment criteria and values as listed in table 1.

The two horizontal components of relative block velocity may be determined by geodesy or by a kinematic model. The fault dip θ and shear modulus μ may be based on local data; however, if these are not available, we recommend for consis-

1. Now at: Jet Propulsion Laboratory.

TABLE 1
Seismicity Parameters for Discrete Faults

Subduction Zone?	Crust Type	Fault Type	Slip Rate, mm a^{-1}	Plate Boundary Analog	<cz>, km*	θ, deg.*	μ, GPa*	m_T^{CMT}*	$\dot{M}_0^{CMT}$, Nms^{-1}*	$\dot{N}_{CMT}$, a^{-1}*	β*	m_c^*	z, km*
Yes	(Mixed)	All (merged)	any	SUB	18	14	49	5.66	2.85×10^{14}	79.7	0.64	9.58	—
No	Continental	Thrust	any	CCB	18	20		5.66	1.06×10^{13}	10.1	0.62	8.46	13
		Strike-slip	any	CTF	8.6	73	27.7	5.66	3.8×10^{12}	7.71	0.65	8.01	12
		Normal	any	CRB	3	55		5.33	1.67×10^{12}	11.1	0.65	7.64	6
	Oceanic	Thrust	any	OCB	3.8	20	49	5.66	4.6×10^{12}	4.57	0.53	8.04	14
		Strike-slip	<39.5	slow OTF	13				6.7×10^{12}	15.5	0.64	8.14	
			39.5–68.5	medium OTF	1.8	73	25.7	5.50	9.4×10^{11}	15.8	0.65	6.55	14
			>68.5	fast OTF	1.6				9.0×10^{11}	14.6	0.73	6.63	
		Normal	any	OSR/normal	eq. (3)	55	25.7	5.33	6.7×10^{11}	16.5	0.92	5.86	8

* Based on Bird and Kagan (2004), table 5.

tency that the values in table 1 be used, as they were previously assumed by Bird and Kagan (2004) in their estimation of $\langle c\,z \rangle$.

Note that a distinction is made between subduction zones (SUB) and all other faults. As in Bird (2003), subduction zones are only those major thrust fault zones that produce Wadati-Benioff zones of intermediate and/or deep seismicity and/or linear volcanic arcs. The Cascadia subduction zone extends into the northern part of the RELM test area. All other faults are classified as being in either oceanic or continental crust. As in Bird (2003), "oceanic" crust is that which has linear magnetic anomalies and/or water depths greater than 2 km; "continental" crust is everywhere else. There is no oceanic crust in the California test area defined by RELM, although it is found in some western portions of the expanded rectangular area of figure 4.

Bird *et al.* (2002) found that oceanic spreading ridges (OSR) have very thin coupled seismogenic lithosphere and that $\langle c\,z \rangle$ decreases exponentially with increasing spreading rate. Based on additional analysis of the OSR/normal-faulting subcatalog of Bird and Kagan (2004), we propose new constants for this empirical relation:

$$\langle c\,z \rangle_{\mathrm{OSR}} \cong (1480\ \mathrm{m}) \exp\left(-\text{spreading rate} / 19\ \mathrm{mm\ a^{-1}}\right) \qquad (3)$$

which is consistent with the global-mean $\langle c\,z \rangle_{\mathrm{OSR}}$ of 130 m found by Bird and Kagan (2004) and with the dip and shear modulus values in table 1.

Table 1 requires that non-SUB faults be classified as thrust, strike-slip, or normal. We classify dipping faults of oblique slip as normal or thrust (according to the sense of the dip-slip component), and assign the default dips appropriate to their sense of dip-slip. However, small components of convergence or divergence across nominally strike-slip faults are acceptable in equation (2) because the default dips suggested in table 1 are not vertical. See Bird and Kagan (2004) for justification.

Once the long-term seismic moment rate ($\dot{M}_0$) of a fault is determined, its expected long-term shallow seismicity rate is obtained in two steps. First, we divide the long-term moment rate by the model moment rate (integral of tapered Gutenberg-Richter distribution of Jackson and Kagan 1999) of the appropriate subcatalog of the Harvard Centroid Moment Tensor (CMT) catalog (as defined by Bird and Kagan 2004), and multiply by the number of events in that subcatalog to determine the rate of earthquakes that will exceed the threshold magnitude of that subcatalog:

$$\dot{N}(m > m_{\mathrm{T}}^{\mathrm{CMT}}) = \left(\dot{M}_0 / \dot{M}_0^{\mathrm{CMT}}\right) \dot{N}^{\mathrm{CMT}}. \qquad (4)$$

Then we adjust the forecast rate to any desired threshold magnitude m_T by using the tapered Gutenberg-Richter model (see also equation (9) of Bird and Kagan 2004):

$$\dot{N}(m > m_T) = \dot{N}(m > m_T^{\mathrm{CMT}}) \left(\frac{M_0(m_T)}{M_0(m_T^{\mathrm{CMT}})} \right)^{-\beta} \times \exp\left(\frac{M_0(m_T^{\mathrm{CMT}}) - M_0(m_T)}{M_0(m_c)} \right) \qquad (5)$$

where m_c is the corner magnitude for seismicity of the analog plate boundary type. All values needed for these computations are included in table 1.

Some readers may be concerned that these equations permit even short faults to generate very large earthquakes. However, it should be remembered that our hypotheses are intended to predict distributions of shallow epicenters and/or hypocenters, and there is no implication that the rupture of a large earthquake would be confined to the fault that generated the hypocenter. Ruptures may percolate along the quasi-fractal network of interconnected faults, or even break new fractures in the lithosphere. This is one fundamental difference between our hypothesis and a strictly "segmented-fault, characteristic-earthquake" type of model. (Another is the integrated, consistent treatment of anelastic strain rates in continua.)

Another point to make about the SHIFT model is that the residual uncertainties in the corner magnitudes for the seven plate settings, and resulting uncertainties in their coupled seismogenic thicknesses, are not a serious source of error. This is because that particular uncertainty is largely self-canceling when we focus on forecasting the numbers of earthquakes rather than their moment rates. Essentially, we could say that in most cases the earthquake rates are scaled from the earthquake rates in the seismic catalogs, using moment rate only as a convenient combination of factors such as fault length, slip rate, dip, rake, elastic modulus, etc. (It would actually be possible to write the hypotheses without referring to moment rate at all, but this would greatly complicate the statement of the hypothesis for seismicity of deforming continua. Also, the error-cancellation does not operate if one computes earthquake rates for very high magnitudes—above the magnitudes of the largest earthquakes in the calibration subcatalog—and therefore such a reformulation would be less general.)

The spatial distribution of the fault-related seismicity forecast by the above equations can be estimated in two alternative ways. (1) Epicenters can be distributed about the fault trace according to empirical spatial probability density functions (B of Bird and Kagan 2004) defined for each plate boundary type. This is most appropriate when a single fault trace is used to represent any and all distributed faults in a plate boundary network, and we always use this method for subduction zones. (2) For individual faults within a complex plate boundary zone or orogen, hypocenters can be distributed evenly on the potentially seismogenic portion of the fault plane, with epicenters projected upward to the surface. In this case, epicenters lie uniformly distributed in a band beside the trace, with width

$$\Delta x = \langle z \rangle \cos\theta \tag{6}$$

using default values of the seismogenic depth $\langle z \rangle$ suggested in table 1 (consistent with table 5 of Bird and Kagan 2004). However, since these were not determined by a global survey as the values of $\langle c\, z \rangle$ were, other depths may be appropriate in particular cases. Since the sense of dip of nominally "vertical" strike-slip faults is generally not known, we distribute epicenters in a band that extends for distance Δx on each side of the trace.

Our forecast for RELM does not include any diffusive smoothing to account for epicenter mislocation; we presume that this will be handled by those who test the forecast in the future.

SEISMICITY OF DEFORMING CONTINUA

The long-term average rate of elastic strains is assumed to be negligible in comparison to the rate of anelastic or permanent strains accumulated by frictional faulting, cold-work plasticity, solution transfer, dislocation creep, and other permanent-strain mechanisms. (The magnitude of possible elastic strain changes is bounded, so as the averaging window becomes longer, the supremum of the absolute value of the mean elastic strain rate declines inversely.) Therefore, we treat the long-term average strain-rate tensor in continua (*i.e.*, the "blocks" between mapped faults) as purely anelastic.

We first find the long-term average strain-rate tensor's three orthogonal principal axes and three principal values: $\dot{\varepsilon}_1 \le \dot{\varepsilon}_2 \le \dot{\varepsilon}_3$. Because all anelastic strain mechanisms conserve volume (to a first approximation, neglecting any changes in porosity), we know that $\dot{\varepsilon}_1 + \dot{\varepsilon}_2 + \dot{\varepsilon}_3 = 0$. This permits the vertical strain rate $\dot{\varepsilon}_{rr}$ (which is equal to one of $\dot{\varepsilon}_1$, $\dot{\varepsilon}_2$, or $\dot{\varepsilon}_3$) to be determined from the two other principal strain rates in the horizontal plane (called $\dot{\varepsilon}_{1h}$ and $\dot{\varepsilon}_{2h}$, with $\dot{\varepsilon}_{1h} \le \dot{\varepsilon}_{2h}$). It also follows that $\dot{\varepsilon}_1 < 0 < \dot{\varepsilon}_3$; only the sign of $\dot{\varepsilon}_2$ can vary. In the seismically coupled portion (fraction c) of the potentially seismogenic or brittle part of the lithosphere (extending to depth z), earthquakes will be generated on minor fault planes that (approximately) bisect the angles between principal long-term strain axes of opposite sign. However, they will not be generated by numerical differences between the two principal long-term strain rates of the same sign. Therefore, in the general case, the continuum will contain two pairs of conjugate fault sets, but not three.

In the computation of our December 2005 forecast for the RELM test, we estimated the seismic moment production of an area A of lithosphere with uniform long-term anelastic strain rate as:

$$\dot{M}_0 = A\langle c\, z \rangle \mu \begin{bmatrix} (\dot{\varepsilon}_3 - \dot{\varepsilon}_1) \\ +(\dot{\varepsilon}_3 - \dot{\varepsilon}_2) \quad \mathrm{IFF}(\dot{\varepsilon}_3\ \dot{\varepsilon}_2 < 0) \\ +(\dot{\varepsilon}_2 - \dot{\varepsilon}_1) \quad \mathrm{IFF}(\dot{\varepsilon}_2\ \dot{\varepsilon}_1 < 0) \end{bmatrix} \tag{7a}$$

However, on later consideration (especially of those cases where $\dot{\varepsilon}_2$ has small magnitude), we decided that equation (7a) is incorrect and that a better estimator is:

$$M_0 = A\langle c\, z \rangle \mu \begin{cases} 2\varepsilon_3; & \text{if } \varepsilon_2 < 0, \textit{ OR} \\ -2\varepsilon_1; & \text{if } \varepsilon_2 \ge 0 \end{cases} \tag{7b}$$

Numerical results quoted below in this paper will be based on equation (7b), which we consider more accurate, even though the forecast submitted in 2005 was based on equation (7a) and cannot be changed. (Fortunately, the difference in overall regional seismicity caused by this change of formula is only –0.5%, because in California continuum seismicity is small compared with fault seismicity.)

Values of coupled seismogenic thickness $\langle c\, z \rangle$ should be taken from table 2. The computation of seismicity rates at various threshold magnitudes follows equations (4) and (5) above, but using the parameter values listed in table 2. The epicenters will be uniformly distributed throughout area A, which in our programs is a spherical-triangle finite element.

TABLE 2
Seismicity Parameters for Volumes with Distributed Anelastic Straining

Crust Type	Vertical Strain Rate	Strain Rate Criterion	Plate Boundary Analog	$\langle cz \rangle$, km*	μ, GPa*	m_T^{CMT}*	$\dot{M}_0^{CMT}$, Nms^{-1}*	$\dot{N}_{CMT}$, a^{-1}*	β*	m_c^*
Continental	$\dot{\varepsilon}_{rr} > 0$	$\dot{\varepsilon}_{rr} > 0.364\ \dot{\varepsilon}_{2h}$	CCB	18	27.7	5.66	1.06×10^{13}	10.1	0.62	8.46
		$\dot{\varepsilon}_{rr} \le 0.364\ \dot{\varepsilon}_{2h}$								
	$\dot{\varepsilon}_{rr} = 0$	—	CTF	8.6	27.7	5.66	3.8×10^{12}	7.71	0.65	8.01
	$\dot{\varepsilon}_{rr} < 0$	$\dot{\varepsilon}_{rr} \ge 0.364\ \dot{\varepsilon}_{1h}$								
		$\dot{\varepsilon}_{rr} < 0.364\ \dot{\varepsilon}_{1h}$	CRB	3	27.7	5.33	1.67×10^{12}	11.1	0.65	7.64
Oceanic	$\dot{\varepsilon}_{rr} > 0$	$\dot{\varepsilon}_{rr} > 0.364\ \dot{\varepsilon}_{2h}$	OCB	3.8	49	5.66	4.6×10^{12}	4.57	0.53	8.04
		$\dot{\varepsilon}_{rr} \le 0.364\ \dot{\varepsilon}_{2h}$								
	$\dot{\varepsilon}_{rr} = 0$	—	slow OTF	13	25.7	5.50	6.7×10^{12}	15.5	0.64	8.14
	$\dot{\varepsilon}_{rr} < 0$	$\dot{\varepsilon}_{rr} \ge 0.364\ \dot{\varepsilon}_{1h}$								
		$\dot{\varepsilon}_{rr} < 0.364\ \dot{\varepsilon}_{1h}$	OCB[sic]	3.8	49	5.66	4.6×10^{12}	4.57	0.53	8.04

* Based Bird and Kagan (2004), table 5.

Table 2 is very similar to table 1, but there are important differences. First, the assignment of the tectonic style as basically thrusting, strike-slip, or normal is based on the magnitude of the vertical principal strain rate relative to the two horizontal principal strain rates. If the absolute value of the vertical strain rate is small relative to horizontal principal strain rates the region is compared with transform plate boundaries. (The exact bounding value of the strain-rate ratio is chosen to be consistent with Bird's [2003] somewhat arbitrary classification of faults as transforms when they lie with 20° of the estimated azimuth of relative plate motion, because this classification of plate boundaries was then used by Bird and Kagan [2004] in their seismicity calibration.) Second, distributed faulting with modest slip on each individual fault (small enough so that no faults are mapped, except at unusually large map scales) will not produce advective structures with disturbed geotherms like midocean spreading ridges or subduction zones. Therefore, all distributed compression in oceanic crust is modeled using the plate boundary analog OCB (oceanic convergent boundary, other than subduction zone). All distributed extension in oceanic crust is also modeled as having the coupled seismogenic thickness of an OCB (rather than the extremely small thickness of OSR). Finally, all distributed strike-slip in oceanic crust is modeled as analogous to slow oceanic transform fault (OTF) boundaries, because the slip rate on each individual fault is expected to be $\ll$ 39.5 mm a^{-1}. The joint implication of these suggested rules is that the corner magnitude for continuum seismicity is hypothesized to be in the range from 7.64 (continental rift boundary [CRB]) to 8.46 (continental convergent boundary [CCB]). As a check on this, we analyzed the plate-interior (INT) subcatalog of CMT earthquakes defined by Bird and Kagan (2004) by maximum-likelihood fitting of a tapered Gutenberg-Richter frequency-magnitude distribution and found that its corner magnitude is greater than 7.6 with 95% confidence. The most important earthquakes determining this conclusion were the 26 January 2001 Gujarat earthquake (*m* 7.66) and the 25 March 1998 earthquake off the margin of Antarctica (*m* 8.12). No upper bound on the corner magnitude could be determined.

THE PROBLEM OF HYPOCENTRAL DEPTH DISTRIBUTION

The method outlined above takes its seismic productivity calibrations from the study of Bird and Kagan (2004), which classified shallow earthquakes (centroid depth ≤ 70 km) in the Harvard CMT catalog. (The Harvard CMT location process does not discriminate between oceanic and continental velocity structures, and its depths are measured from a reference spheroid close to sea level and/or the geoid.) Therefore, the forecasts outlined above are for shallow seismicity, with centroid depths no more than 70 km below sea level.

However, for the RELM test (Schorlemmer *et al.* 2007, this issue), it is necessary to prepare forecasts of seismicity with hypocentral depths of no more than 30 km. In future calculations of seismic hazard it will also be necessary to forecast the detailed depth distributions.

Our initial hope was that the centroid depths in the Harvard CMT catalog might be precise enough to serve this purpose, so that the detailed depth distribution for any fault or continuum region might be taken to be the depth distribution of the most comparable plate-boundary subcatalog of Bird and Kagan (2004). However, a large fraction of shallow CMT events (about one-quarter to one-third of those above magnitude 5.66) are reported to have centroid depth of 15 km, which is the value at which the iteration of the location was started.

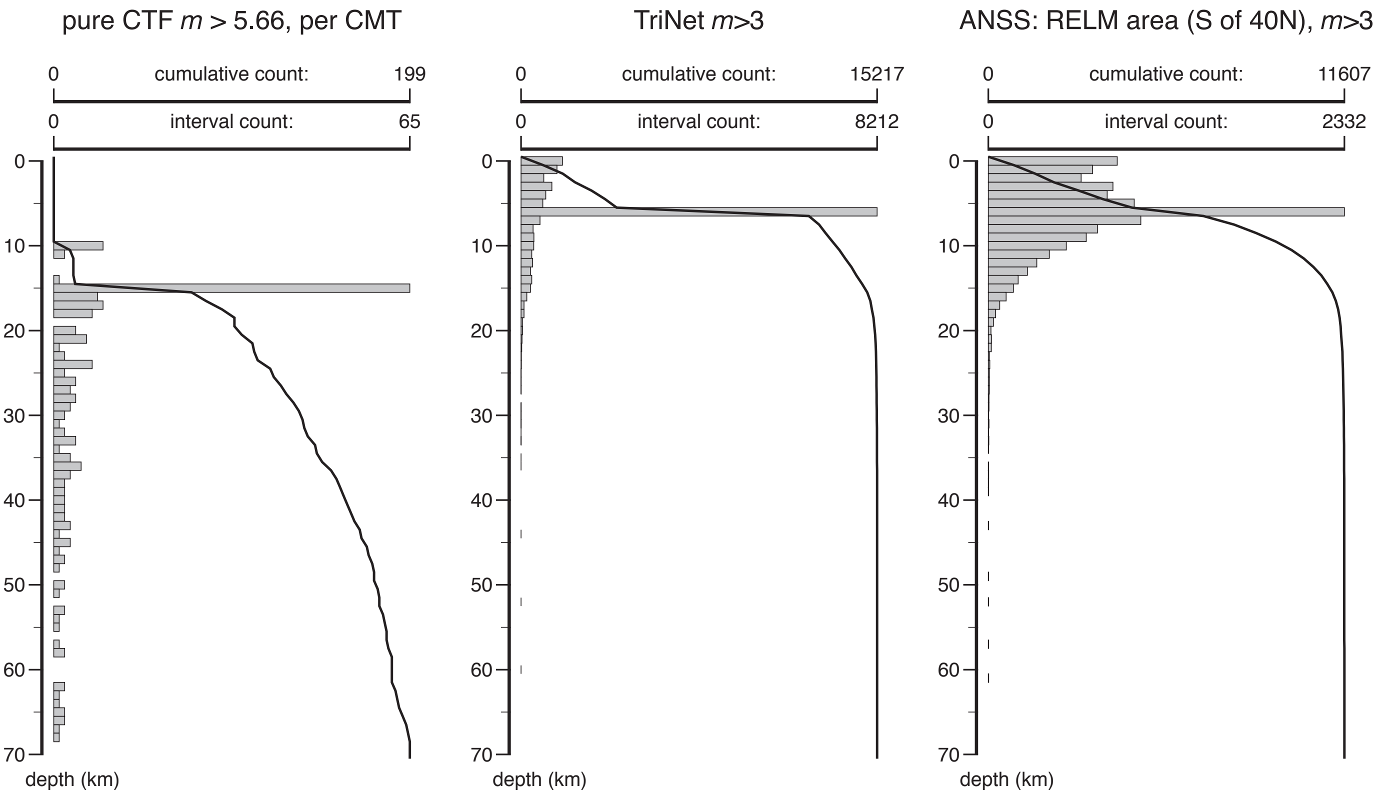

▲ **Figure 1.** Comparison of teleseismic-network versus local-network depth distributions of events within the "shallow" domain of 0~70 km below sea level, for continental settings dominated by strike-slip faulting. At left, histogram and cumulative distribution of centroid depths from the global CTF subcatalog of the Harvard CMT catalog, as selected by Bird and Kagan (2004). Center, histogram, and cumulative distribution of hypocenter depths from the TriNet catalog in the southern California region. Right, histogram and cumulative distribution of hypocenter depths from the ANSS catalog in California south of 40°N (excluding the Cascadia subduction zone). While the two local catalogs agree, the global teleseismic catalog probably gives an inaccurate representation of the depth distribution.

Second, CMT centroid depths are never permitted to be less than 10 km, possibly to avoid the embarrassment of locating a centroid in the ocean. Figure 1 shows the histogram of centroid depths for threshold $m > 5.66$ from the continental transform fault (CTF) subcatalog of Bird and Kagan (2004), compared with two local California catalogs. (These California catalogs were windowed so as to exclude the Cascadia subduction zone and are evaluated at a lower threshold of $m > 3$.) The mismatch is striking; in particular, the CTF subcatalog of CMT indicates that 94% of shallow centroids are at 15 km or deeper, while the southern California TriNet catalog indicates that 96% of hypocenters are 14 km or shallower. The Advanced National Seismic System (ANSS) catalog agrees with TriNet, indicating 95% of hypocenters are 14 km or shallower.

Our second attempt was to use relocated hypocenters for the events in the CTF subcatalog of the CMT catalog. These relocations were taken from the centennial catalog of Engdahl and Villaseñor (2002), which includes relocations of many large events during 1956–1999. Because of the switch from centroid to hypocenter times and locations, a flexible matching criterion was used, permitting matches up to 60 s apart in time, 0.9 apart in magnitude, and 180 km apart in the horizontal plane. We found it was possible to match 147 out of 199 (74%) of the CMT/CTF events with $m > 5.66$, and the results are shown in figure 2. Still, 81% of the events are located at 15 km or deeper, which is an unacceptably poor match to the two California catalogs shown in figure 1.

In another similar comparison, we looked at shallow seismicity of subduction zones. We matched shallow subduction zone events from the SUB subcatalog of CMT to the centennial catalog of Engdahl and Villaseñor (2002), with success in 1,581 out of 2,090 events with $m > 5.66$ (76%). For comparison, we sampled the ANSS catalog in the Cascadia region of 126~120°W, 40~43°N at the lower threshold of $m > 3$. (Admittedly, this sample from ANSS includes triple-junction seismicity as well as Cascadia subduction zone activity.) Again, the depth distributions were unacceptably different (figure 3). For example, the centennial catalog shows 51% of the shallow events as deeper than 30 km, while in the ANSS catalog this fraction is only 6%.

It is possible that these mismatches indicate some fundamental problem with our approach, in the sense that California could conceivably have hypocentral depth distributions completely different from those of other CTF and SUB boundar-

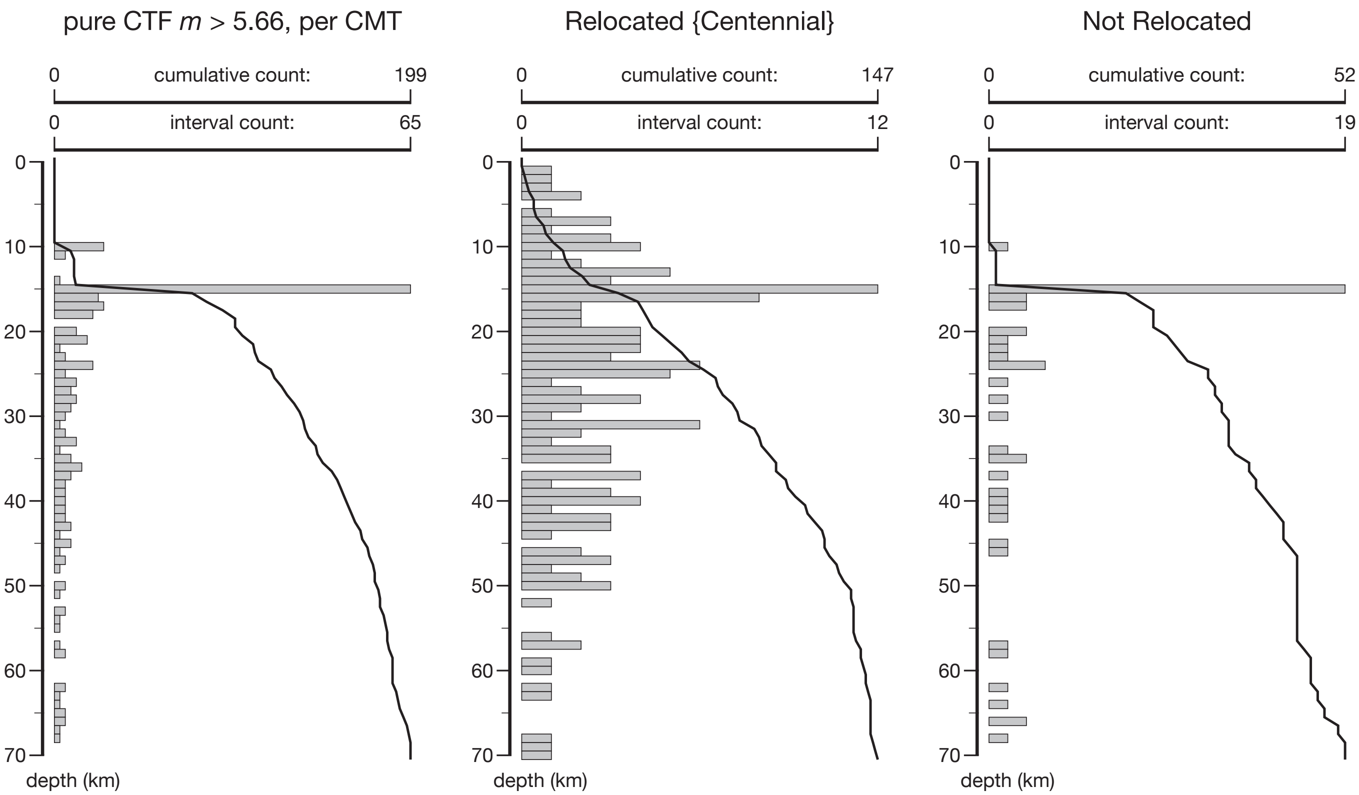

▲ **Figure 2.** An attempt to improve the teleseismic resolution of event depths by matching Harvard CMT events with Engdahl and Villaseñor (2002) hypocenter locations of continental transform earthquakes. At left is the same CTF subcatalog of CMT seen in figure 1. Center, depth distribution of Engdahl and Villaseñor (2002) hypocenter locations for those events that could be matched between catalogs. Right, depth distribution of residual CMT/CTF events that could not be matched in the hypocenter catalog. Because even the "corrected" depth distribution at center is still very different from local-catalog depth distributions of continental transform tectonics in California (seen at center and right of figure 1), we consider this procedure to be unsuccessful. The difference between the depth distributions of two teleseismic catalogs is small compared with the difference between the depth distributions of teleseismic and local catalogs.

ies around the world. However, we prefer to interpret these problems as artifacts of poor depth resolution in all teleseismic catalogs. Consequently, we recommend that where accurate local catalogs exist, these catalogs should be used to forecast the details of depth distributions within the "shallow" domain of 0 to 70 km depth. In some cases, this will require using a lower threshold for determining the depth distribution than the threshold used in making the forecast.

IS A LONG-TERM AVERAGE SHIFT MODEL TESTABLE?

The preceding paragraphs and equations (together with tables 1 and 2) outline a model of long-term shallow seismicity. For brevity, this collection of equations, decision rules, and parameters may be called the SHIFT model. To help resolve any remaining ambiguities, we provide the FORTRAN 90 code for the program Long_Term_Seismicity, which we used to implement these methods:

ftp://element.ess.ucla.edu/Long_Term_Seismicity/Long_Term_Seismicity.f90

In a procedural sense the SHIFT model is testable because we have met the format and deadline requirements for the five-year RELM test described in this volume. We strongly support systematic scoring of forecasts that have been converted to common format by impartial referees who follow pre-established procedures.

However, our submission does not imply that we expect the SHIFT model to outperform catalog-based (and therefore time-dependent) models in a five-year test. The existence of "legacy" aftershock swarms, not considered in our model, gives a large advantage to our competitors in any short-term test. Rather, we expect that the SHIFT model (and other similar long-term average models) will become relatively more valuable as the length of the testing period is increased and the legacy aftershock swarms are gradually submerged in background seismicity and new swarms. With this contribution we merely begin a lengthy process of learning the time-window at which

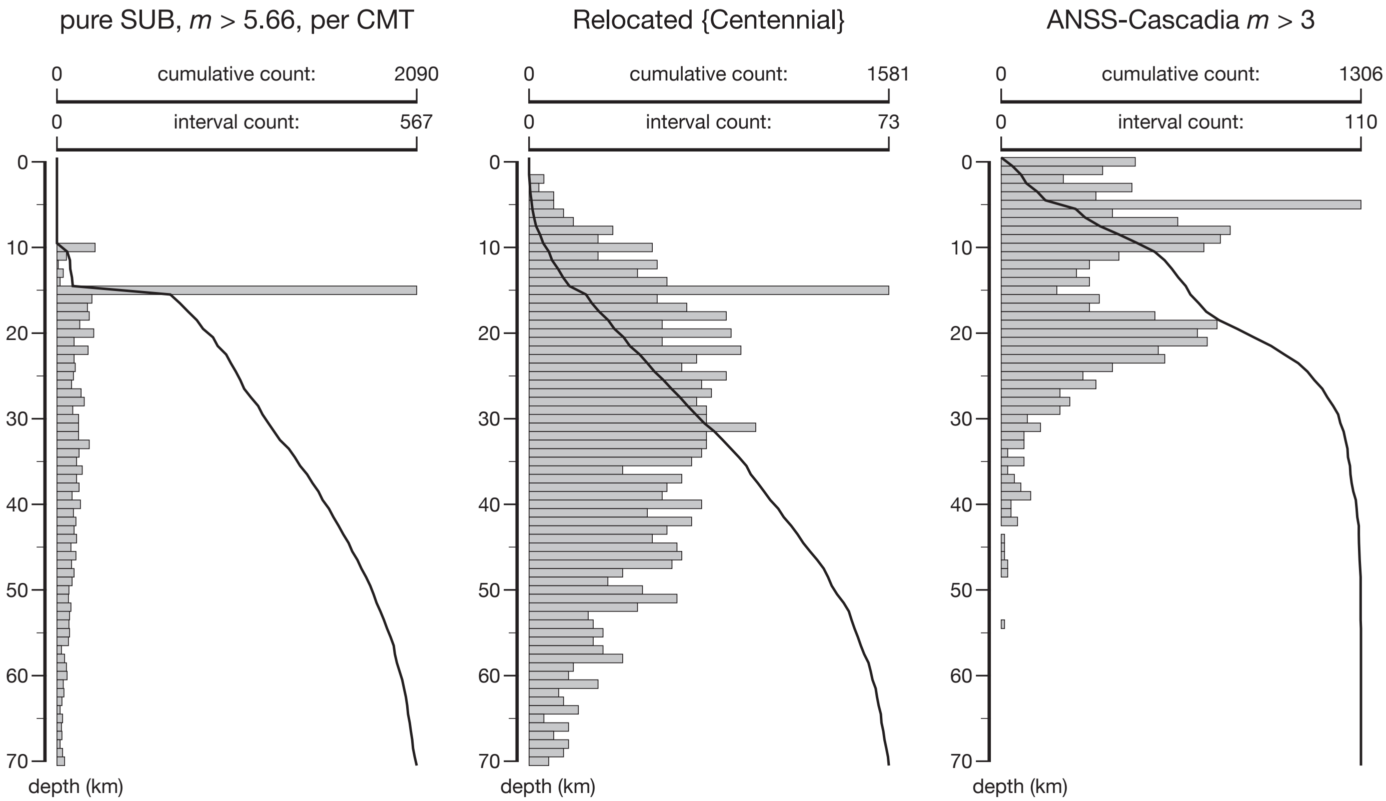

▲ **Figure 3.** Comparison of two teleseismic-network depth distributions for shallow subduction zone seismicity with a representative local-network depth distribution. At left, histogram and cumulative distribution of centroid depths from the global subduction zone (SUB) subcatalog of the Harvard CMT catalog, as selected by Bird and Kagan (2004). Center, depth distribution of Engdahl and Villaseñor (2002) hypocenter locations for those CMT/SUB events that could be matched between catalogs. Right, depth distribution of ANSS local-network hypocenter locations from the Cascadia region (126~120°W, 40~43°N) in northwest California. Either version of the teleseismic depth distribution is biased too deep, if judged by the standard of the local-network depth distribution.

this transition in optimal forecasting strategy might occur (and how it might depend on forecast area, threshold magnitude, level of tectonic activity, etc.). We hope that the end of the five-year RELM test will be followed by the initiation of a 50-year test (more appropriate to the concerns of architects), which is then followed by a 500-year test, and so on.

This discussion begs the question: Is the SHIFT model testable in an absolute sense (not relative to other forecasts) and, if so, how? A simple answer is provided by our definition of "long-term" as 10^4~10^6 years (see ftp://element.ess.ucla.edu/NeoKinema/Appendix-Algorithm_of_NeoKinema.pdf). Therefore, a SHIFT forecast can be evaluated in any region (however small) by a 10,000-year test. A more satisfying answer is that provisional tests can be conducted in shorter times if the geographic scope is widened and if one supplementary hypothesis is accepted. This would be the "ergodic assumption" that, for studies of globally uncorrelated behavior, data collected widely in space can substitute for local data collected over long times. Physically, we believe that local regions depart from their long-term average seismicity primarily because of regional increases or decreases in elastic strain. (For example, geodesy has detected such strain accumulation around the Cascadia subduction zone, much of which has been locked since A.D. 1700.) If individual plate boundaries that experience such variations are not coordinated in their behavior, then a regional or global test should be less strongly affected by changes in elastic strain than a local test. Consequently, we also call for the establishment of systematic global testing of seismic forecasts.

Even if the ergodic assumption were proven inapplicable to this problem so that the SHIFT forecasts were not testable (in one lifetime) as scientific predictions, the SHIFT forecasts might still be perceived as having value as plausible estimates for use in engineering of buildings and public policy. Such estimates are needed by those who design dams and nuclear waste repositories for very long service lives. Ideally, they should also be considered by those who design dwellings, since the European experience is that a small fraction of dwellings will still be in service after 300~500 years.

SOURCES OF KINEMATIC INFORMATION FOR SHIFT MODELS

Because we anticipate that global tests will be important for the validation of the SHIFT model, we have designed the model to be extremely flexible in accommodating almost any kind of kinematic description of the long-term average velocity field of the Earth's surface. The SHIFT model can be used to forecast long-term seismicity from rigid-block (plate or microplate) models of the lithosphere, by use of equations (1)–(6) and table 1. Or, the SHIFT model can be used to forecast long-term seismicity from continuum models of the lithosphere, by use of equations (4)–(7) and table 2.

Our preference is for mixed models that include both fault slip and anelastic deformation of the intervening lithosphere. Kong (1995; see also Kong and Bird 1996) used finite element models to simulate both kinds of neotectonic deformation in Asia and found that in the best model the straining due to fault slip was 69% of the total, while that due to anelastic continuum deformation was 31%. Finite elements are an appropriate numerical tool because F-E grids always allow for continuum deformation, while degrees of freedom associated with faulting can be represented by locally concentrated nodes and/or special elements. For purposes of interfacing with the SHIFT model, it is not necessary for the F-E grid to be 3-dimensional; because only surface velocities are required, 2-D planar or spherical-shell grids are adequate.

Finite-element models of neotectonics may be either dynamic ("forward") models or kinematic ("inverse") models. Dynamic models (such as our program Shells) use velocity and/or traction boundary conditions and assumed anelastic rheologies and solve the momentum equation. Kinematic models (such as our program NeoKinema) accept only velocity boundary conditions, and fit the internal velocity field to available data (and *a priori* constraints) by weighted least-squares or other statistical means. While dynamic models are better for generating physical insight, they rarely match more than a fraction of fault slip-rate and geodetic data within their uncertainties. Kinematic models are better for seismicity forecasting because they can usually be weighted so as to fit all data reasonably well (unless the data sets are internally or mutually inconsistent).

KINEMATIC FINITE-ELEMENT PROGRAM NEOKINEMA

Our program NeoKinema represents a further development of methods first used in palinspastic kinematic F-E program Restore (Bird 1998). Its equations and methods cannot be described fully in this paper but are available in a 27-page appendix at ftp://element.ess.ucla.edu/NeoKinema/Appendix-Algorithm_of_NeoKinema.pdf, and a full-length paper with extensive graphics and sample files is in preparation.

The model domain is the area within a closed curve on the Earth's spherical surface. The domain is divided into many spherical-triangle finite elements (Kong and Bird 1995), with nodes at their corners. The degrees of freedom are two at each node: a southward component of long-term-average velocity and an eastward component of long-term average velocity. (Therefore, differentiation of velocity within each triangle yields the long-term average strain rate, which is anelastic by definition.) Vertical velocity components are not modeled.

The general formalism for solving for nodal velocities is to minimize a weighted least-squares objective function by finding its stationary point in multidimensional velocity-component space with a system of linear equations. Nonlinearities are handled by iteration of the solution. Velocity boundary conditions are typically applied all around the edges of the models, which should ideally lie within the relatively rigid parts of surrounding plates.

Geodetic benchmarks are treated as internal point constraints on the velocity field (with associated uncertainties). However, geodetic velocities are first "corrected" to remove local elastic bending due to temporary locking of the seismogenic portion of faults, using the current model estimates of the fault slip rates, locking depths assigned *a priori*, and analytic solutions for rectangular dislocations in a uniform elastic half-space. This requires iteration. If a full covariance matrix for geodetic velocity components is available, we attempt to minimize $(\vec{m}-\vec{g})^T\,\tilde{N}(\vec{m}-\vec{g})$, where $\vec{m}$ is the vector of model velocity components, $\vec{g}$ is the vector of geodetic velocity components, and $\tilde{N}$ is the normal matrix (inverse of the covariance matrix of the geodetic velocity components).

Faults with positive target slip rates contribute to the target strain rates of all elements they cut through. Uncertainties in fault slip rates contribute to anisotropic compliance of all elements that the faults cut through. An unlimited number of faults can cut through any element, as long as no node lies exactly on a fault trace. (However, better accuracy is expected when major faults are outlined by narrow quadrilaterals formed of pairs of elongated triangular elements.) Input fault slip rates can be heave rates or throw rates, whichever is available. Throw rates are converted into heave rates using the default fault dips (table 1). Dip-slip faults can be permitted to slip obliquely (using a control parameter) for more realistic flexibility of the fault network. This also requires iteration of the solution.

In elements with no mapped fault traces ("continuum elements") the horizontal principal directions of the long-term anelastic strain rate are constrained by horizontal principal stress directions, which are interpolated from data of the World Stress Map into every finite element by the method of Bird and Li (1996). Unfaulted elements have a nominal strain rate of zero, with an assigned uncertainty. This uncertainty (parameter μ at ftp://element.ess.ucla.edu/Long_Term_Seismicity/Long_Term_Seismicity.f90) can be obtained in bootstrap fashion by iteration of the entire solution.

There are two "tuning" parameters: (1) relative weight of trace-based geologic data; and (2) relative weight of area-based stiffness and isotropy constraints (both relative to constant weight of point-based geodetic data). These are expressed through dimensional, user-selected input parameters called the "reference length" L_0 and the "reference area" A_0. Loosely speaking, geologic slip rate constraints for each fault trace length of L_0 have about the same weight in the objective function as a single geodetic benchmark with known velocity, and the same weight as the continuum-stiffness and isotropy constraints from an area A_0 of continuum. (Of course, weighting also includes the inverse-square of the standard deviation of each constraint, when expressed as a velocity component.)

APPLICATION TO CALIFORNIA

The finite-element grid used in this calculation (GCN8p6.feg) has 5,243 nodes and 10,233 elements and covers the whole Gorda-California-Nevada orogen as defined by Bird (2003).

Velocity boundary conditions are applied on all edges, using North America, Pacific, and Juan de Fuca rotation vectors from model PB2002 of Bird (2003), which in turn was taken from the NUVEL-1 model of DeMets *et al.* (1990) and its NUVEL-1A update (DeMets *et al.* 1994).

The geodetic data are a compilation of 1,021 benchmarks in the western United States, assembled by Zhen-Kang Shen in 2002. These include the southern California benchmarks of the Southern California Earthquake Center (SCEC) Crustal Motion Model v3.0 (Shen *et al.* 2003) and also published velocities from northern California, Nevada, Utah, Oregon, and Washington. Benchmarks less than 2 km from active faults were deleted, because at smaller distances our F-E grid GCN8p6.feg interpolates and smears the fault discontinuities in long-term velocity. No covariance matrix was available, so the error ellipses of different benchmarks were treated as independent.

Stress directions were downloaded from the World Stress Map Project (Reinecker *et al.* 2004), with 963 directions from inside the Gorda-California-Nevada orogen and an additional ~1,000 around its margins used for the interpolation of principal stress directions.

The active and potentially active faults in the Gorda-California-Nevada orogen number at least 690, which include all faults used in the California Geological Survey model of Petersen *et al.* (1996). One of us (P.B.) has maintained a collection of active fault traces and references on geologic slip rates for 20 years, and this was used to supply estimated slip rates and their uncertainties. Admittedly, this collection is very incomplete. The merging of different estimates for a single fault was not automated and therefore was subjective and not strictly reproducible. We have also found, in hindsight, that many of the uncertainties in slip rate we took from tertiary sources are extremely subjective and in need of revision. Future efforts will focus on improving this data set. However, when a geologic fault slip rate is too low, NeoKinema will tend (because of geodetic constraints) to supply the necessary deformation as distributed strain in the vicinity of the trace. Then, our SHIFT model makes little distinction between fault slip and distributed shearing of equal seismic moment rate, so to a first approximation the number of forecast earthquakes at each magnitude is preserved. Our brief comments below will concentrate on total earthquake counts rather than details of the map pattern of the forecast.

This SHIFT forecast is based on the velocity solution of NeoKinema v2.0 model GCN2004084, which was run for 40 iterations with weights $L_0 = 1000$ m and $A_0 = 4 \times 10^8$ m^2, and parameters $\mu = 1 \times 10^{-15}$ s^{-1}, $\xi = 3.2 \times 10^{-17}$ s^{-1}, assumed locking depths of 1~12 km for interplate faults and 14~40 km for the Cascadia subduction zone, and allowing oblique rotations of dip-slip vectors with standard deviation of 20°. These two weights and parameter μ were the result of systematic optimization tests totaling 83 trials and permitted all data sets to be fit reasonably well. Geodetic velocities were fit with root mean square (RMS) relative error of 2.5 standard deviations. Interpolated stress directions were fit with RMS relative error of 2.4 standard deviations. Fault slip rates were fit with RMS relative error of 0.3 standard deviations. (This good fit is somewhat misleading because both relative and absolute misfit concentrated along the San Andreas fault where input uncertainties were largest; however, mean absolute error along the San Andreas was only 4 mm/a.) Continuum deformation had mean absolute value of 6×10^{-16} s^{-1} and RMS value 1.5×10^{-15} s^{-1}, consistent with the assumed μ. All input and output files are available by request.

FORECAST SEISMICITY AND RETROSPECTIVE COMPARISONS

Long-term seismicity forecasts (including aftershocks without distinction) have been computed for threshold magnitudes from 4.95 (in 0.1 steps) to 8.95, in the 0.1° cells of the RELM test template, and the results have been reported for a five-year test. As explained above, we rely on the local TriNet and ANSS catalogs for the depth distributions of seismicity within the "shallow" domain of 0~70 km. Consequently we attribute 94% of forecast shallow SUB seismicity (in the Cascadia region) to depths of 30 km or less, and we attribute 99.9% of forecast shallow CTF, CCB, and CRB seismicity (in the rest of California) to depths of 30 km or less. Figure 4 shows a map of the logarithm of forecast seismicity at threshold magnitude 5.663.

In the geographic rectangle 31.5~43N, 113.1~125.4W surrounding California, our forecast of 63 $m > 5.663$ earthquakes per 25.75 years at centroid depth ≤ 70 km exceeds the Harvard CMT catalog count of 48 events in 1977.01~2002.09, seen in figure 5. (For this comparison we extend the depth range beyond the 0~30 km range of the RELM test, because as we have seen above the Harvard CMT catalog does not reliably place events on the correct side of 30-km depth. Like all numerical results quoted in this section, these seismicity forecasts are based on improved equation (7b) for continuum seismicity, even though the forecast submitted in 2005 for the RELM test was based on equation (7a); the difference is only 0.5%.)

In the slightly smaller RELM test area, for depths of 0~30 km, our forecast of 233 $m > 4.95$ earthquakes per 21 years exceeds the ANSS catalog count of 164 for 1984.01~2004.12. (The spatial pattern of shallow ANSS events, down to magnitude 3, can also be seen in figure 5.)

In the smaller rectangle 32.5~36N, 115~121W in southern California, for depths of 0~30 km, our forecast of 314 $m > 5$ events per 72.67 years is more than twice the TriNet catalog count of 147 for 1932.01~2004.08.

We suggest that California, and especially southern California, may be temporarily below long-term seismicity because of the recent lack of great earthquakes (such as those of 1700, 1857, 1872, and 1906) which might be expected to stimulate numerous magnitude-5+ aftershocks. Alternative explanations include a computational error in our work or a failure of

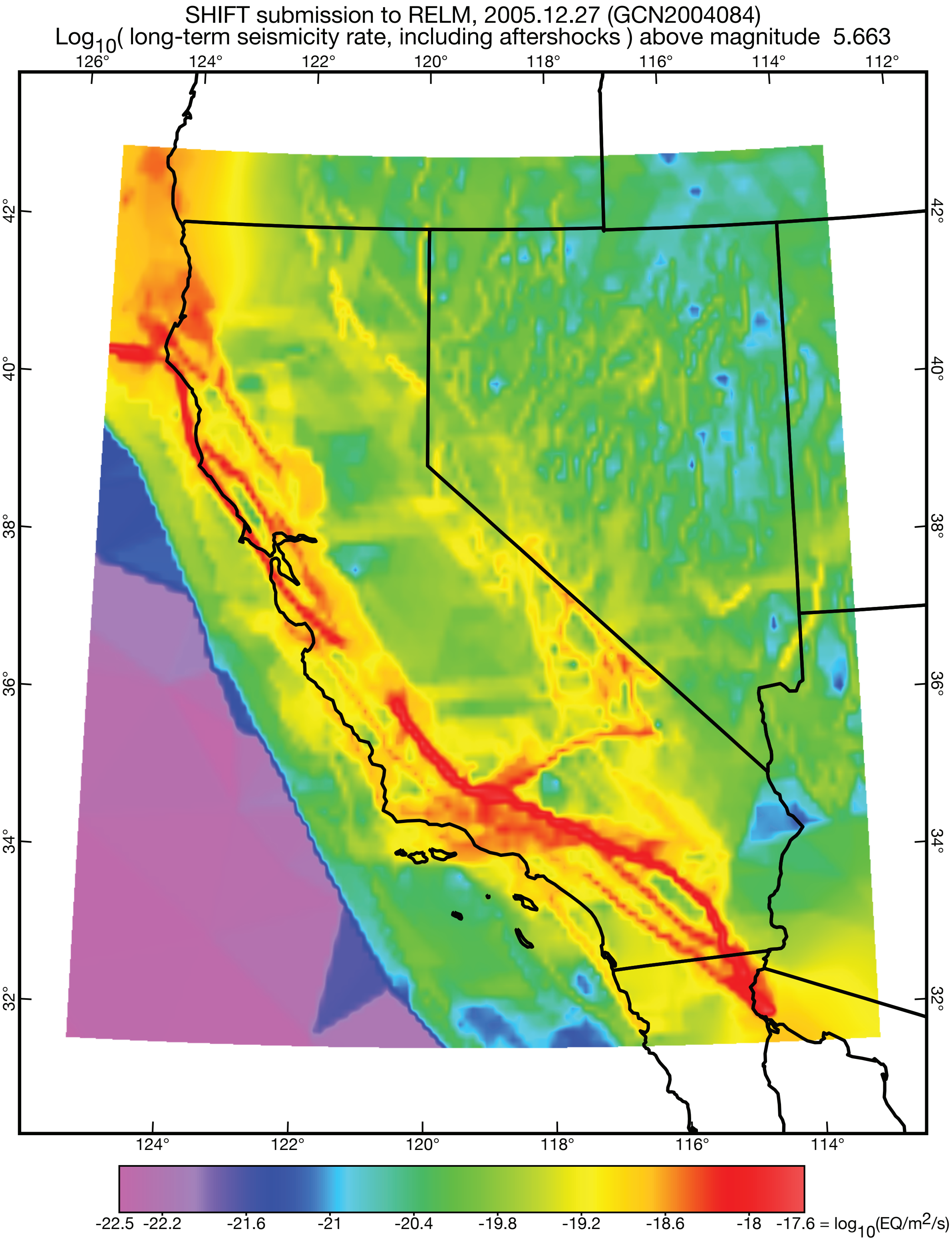

▲ **Figure 4.** Common logarithm of forecast long-term seismicity (in epicenters per square meter per second, including aftershocks) in the California region for threshold magnitude 5.663, according to the SHIFT model. Seismicity in California and surrounding regions (with short-wavelength structure) is based on kinematics from NeoKinema model GCN2004084, as described in the text. Deep-sea seismicity and southern Arizona seismicity are based on strain rates from Shells model Earth5-013. The spatial integral of the forecast rate is equivalent to 63 earthquakes per 25.75 years in the depth range 0~70 km. (To convert seismicity from earthquakes/m^2/s to earthquakes/km^2/year, add 13.5 to the values along the scale. To convert to earthquakes/(100 km)^2/century, add 19.5.)

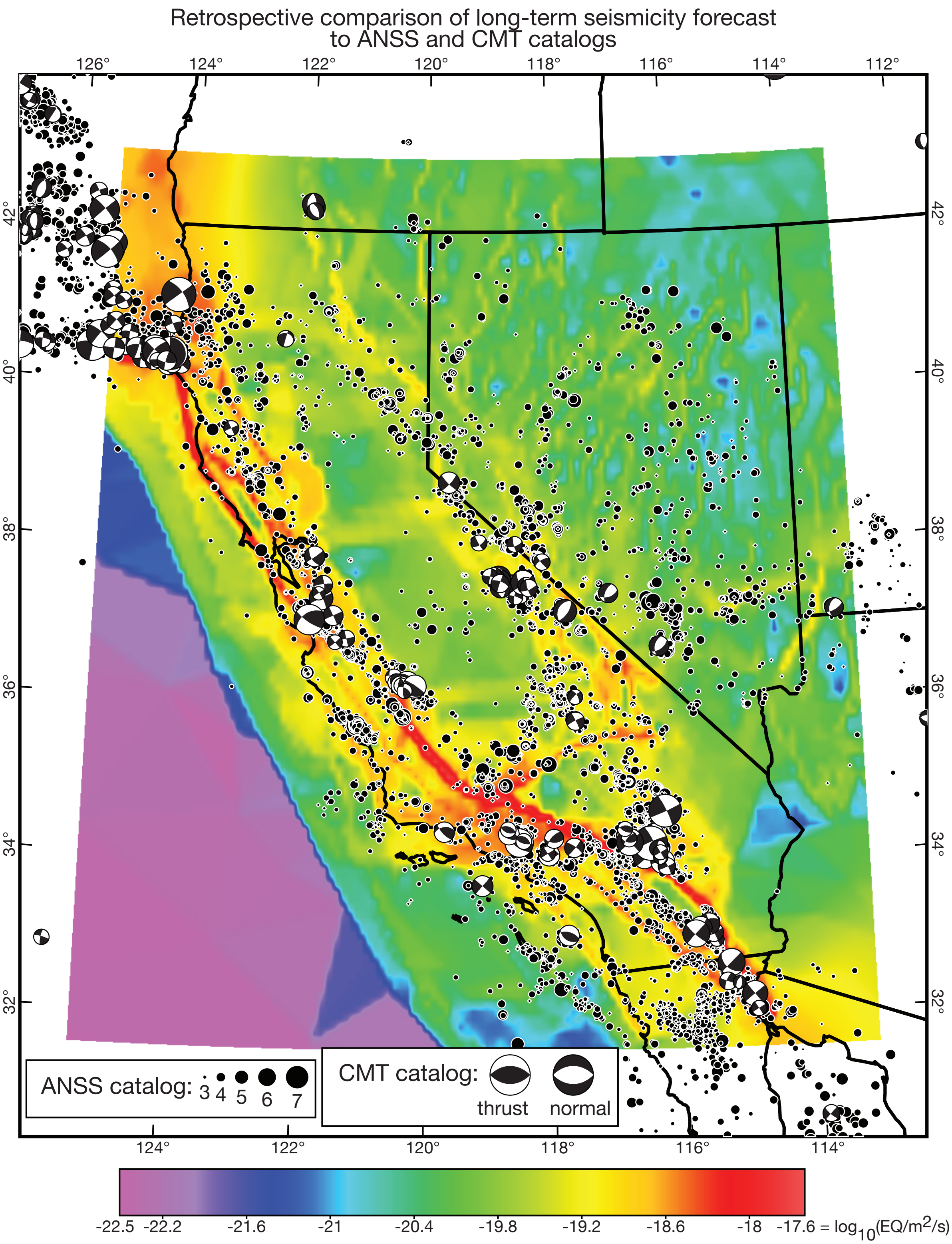

▲ **Figure 5.** Colored background shows long-term forecast, exactly as in figure 4. For retrospective comparison, the Harvard CMT catalog shows 48 events ("beachballs") with $m > 5.663$ at 0~70 km depth in the 25.75 year interval 1977.01~2002.09. Black dots show shallow earthquakes with $m > 3$ in 1984~2004 from the ANSS catalog.

the SHIFT model. Prospective tests in California and other regions (especially those covering longer times and larger regions) may resolve this.

ACKNOWLEDGMENTS

This research was supported by the Southern California Earthquake Center. SCEC is funded by NSF Cooperative Agreement EAR-0106924 and USGS Cooperative Agreement 02HQAG0008. The SCEC contribution number for this paper is 926. Publication supported by the National Science Foundation under grant EAR-0336950. The views and conclusions contained in this document are those of the authors and should not be interpreted as necessarily representing the official policies, either expressed or implied, of the U.S. government.

REFERENCES

Bird, P. (1998). Kinematic history of the Laramide orogeny in latitudes 35°–49° N, western United States. *Tectonics* **17**, 780–801.

Bird, P. (2003). An updated digital model of plate boundaries. *Geochemistry, Geophysics, Geosystems* **4** (3), 1,027, doi:10.1029/2001GC000252.

Bird, P., and Y. Y. Kagan (2004). Plate-tectonic analysis of shallow seismicity: Apparent boundary width, beta, corner magnitude, coupled lithosphere thickness, and coupling in seven tectonic settings. *Bulletin of the Seismological Society of America* **94** (6), 2,380–2,399, plus electronic supplement.

Bird, P., Y. Y Kagan, and D. D. Jackson (2002). Plate tectonics and earthquake potential of spreading ridges and oceanic transform faults. In *Plate Boundary Zones*, ed. S. Stein and J. T. Freymueller, *Geodynamics Series* **30**, 203–218. Washington, DC: American Geophysical Union.

Bird, P., and Y. Li (1996). Interpolation of principal stress directions by nonparametric statistics: Global maps with confidence limits. *Journal of Geophysical Research* **101**, 5,435–5,443.

DeMets, C., R. G. Gordon, D. F. Argus, and S. Stein (1990). Current plate motions. *Geophysical Journal International* **101**, 425–478.

DeMets, C., R. G. Gordon, D. F. Argus, and S. Stein (1994). Effect of recent revisions to the geomagnetic reversal time scale on estimate of current plate motions. *Geophysical Research Letters* **21**, 2,191–2,194.

Engdahl, E. R., and A. Villaseñor (2002). Global seismicity: 1900–1999. In *IASPEI Handbook of Earthquake and Engineering Seismology*, ed. W. H. K. Lee, P. Jennings, H. Kanamori, and C. Kisslinger, 665–690. Amsterdam and Boston: Academic Press.

Jackson, D. D., and Y. Y. Kagan (1999). Testable earthquake forecasts for 1999. *Seismological Research Letters* **70**, 393–403.

Kong, X. (1995). Numerical modeling of the neotectonics of Asia: A new spherical shell finite element method with faults. Ph.D. dissertation, University of California-Los Angeles.

Kong, X., and P. Bird (1995). Shells: A thin-shell program for modeling neotectonics of regional or global lithosphere with faults. *Journal of Geophysical Research* **100**, B11, 22,129–22,131.

Kong, X., and P. Bird (1996). Neotectonics of Asia: Thin-shell finite-element models with faults. In *The Tectonic Evolution of Asia*, ed. A. Yin and T. M. Harrison, 18–34. Cambridge: Cambridge University Press.

Petersen, M. D., W. A. Bryant, C. H. Cramer, T. Cao, M. Reichle, A. D. Frankel, J. J. Lienkemper, P. A. McCrory, and D. P. Schwartz (1996). *Probabilistic Seismic Hazard Assessment for the State of California*. California Department of Conservation, Division of Mines and Geology Open-File Report 96-08.

Reinecker, J., O. Heidbach, M. Tingay, P. Connolly, and B. Müller (2004). The 2004 release of the World Stress Map (available online at http://www.world-stress-map.org).

Schorlemmer, D., M. C. Gerstenberger, S. Wiemer, D. D. Jackson, and D. A. Rhoades (2007). Earthquake likelihood model testing. *Seismological Research Letters* **78** (1), 30–36.

Sornette, D., and V. Pisarenko (2003). Fractal plate tectonics. *Geophysical Research Letters* **30** (3), 1,105, doi:10.1029/2002GL015043.

Shen, Z.-K., D. C. Agnew, R. W. King, D. Dong, T. A. Herring, M. Wang, H. Johnson, G. Anderson, R. Nikolaidis, M. van Domselaar, K. W. Hudnut, and D. D. Jackson (2003). The SCEC Crustal Motion Map, Version 3.0, Southern California Earthquake Center, Los Angeles, http://epicenter.usc.edu/cmm3/ .

Department of Earth and Space Sciences
University of California
Los Angeles, California 90045 USA
pbird@ess.ucla.edu
(P.B.)

Jet Propulsion Laboratory, M/S 300-233
California Institute of Technology
4800 Oak Grove Drive
Pasadena, California 91109 USA
zliu@mail.jpl.nasa.gov
(Z.L.)